RSC Advances

ROYAL SOCIETY OF CHEMISTRY

www.rsc.org/advances

Graphic abstract

We first synthesized N-doped graphene aerogels (NGAs) by using graphene oxide (GO) and melamine via a self-assembly process by one-pot hydrothermal method. The microstructure, surface area and capacitance of NGAs could be facilely controlled by the change of melamine/GO mass ratio. The synthesized NGA-3 exhibited excellent specific capacitance and electrochemical stability.

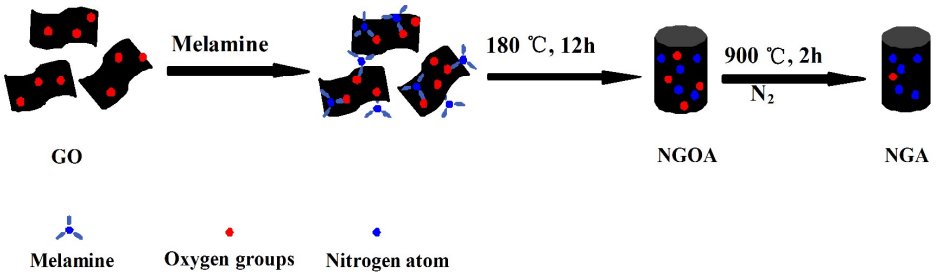

Facile Synthesis of Structure-controllable, N-doped Graphene Aerogels and Their Application in Supercapacitors

Xianpan Shi[1,2,3], Jiayi Zhu[3], Yong Zhang[2], Shuaijie He[1,2,3], Yutie Bi[2], Lin Zhang[1,2,3*]

(1. School of Material Science and Enginnering, Southwest University of Science and Technology, Mianyang 621010, China;

2. Joint Laboratory for Extreme Conditions Matter Properties, Southwest University of Science and Technology and Research Center of Laser Fusion, China Academy of Engineering Physics, Mianyang 621010, China;

3. Research Center of Laser Fusion, CAEP，Mianyang 621900, China)

*Corresponding author. Tel/Fax: +86-0816-2491228. E-mail: zhlmy@sina.com

Abstract: N-doped graphene aerogels (NGAs) were first synthesized by using graphene oxide (GO) and melamine via a self-assembly process by one-pot hydrothermal method. The morphology and structure of the as-prepared materials were characterized by means of scanning electron microscopy, transmission electron microscopy, X-ray diffraction, XPS spectroscopy and nitrogen adsorption/desorption measurement. The electrochemical performance of NGAs were studied by cyclic voltammetry, galvanostatic charge/discharge and impedance spectroscopy measurements. Importantly, the microstructure, surface area and capacitance of NGAs could be facilely controlled by the change of melamine/GO mass ratio. Compared with the pure graphene aerogel (80 F/g at 0.5 A/g), NGA-3 with the mass ratio of 1/15 displayed enhanced specific capacitance (116 F/g) and retained 94 % of the initial capacitance after 1000 cycles. It provided a possible way to obtain graphene based materials with high surface area and capacitance.

Key words: N-doped graphene aerogels; melamine; self-assembly; hydrothermal method; electrochemical performance

1. Introduction

Graphene, a flexible two-dimensional monolayer of sp^2-hybridized carbon atoms, has received tremendous attention in supercapacitors,[1] field-effect transistors,[2] lithium ion batteries,[3] electrochemical biosensor,[4] catalyst carriers,[5] solar cells[6] and so on. Aerogels are a kind of porous materials with ultralow density, high porosity and large surface areas. They could be used in many fields including thermal insulation, hydrogen storage and adsorbents

for toxic ionic or organics.[7, 8] Graphene aerogels permit the individual graphene sheets into three-dimensional (3D) porous skeleton. This combines the unique nanoscale porous structure of the aerogel to graphene, which would improve the feasibility of graphene for the absorption, catalytic, and electrochemical performance. Worsley reported a unique method to prepare graphene aerogels by the reaction of resorcinol-formaldehyde resol and graphene oxide (GO). The obtained graphene aerogel had a low density approaching 10 mg cm^{-3} and a high surface area of 584 m^2/g.[9] Shi first reported a convenient one-step hydrothermal method to prepare a self-assembled graphene hydrogel, which had potential applications in the fields of biotechnology and electrochemistry such as drug-delivery, tissue scaffolds, bionic nanocomposites, and supercapacitors.[10] Han prepared a novel graphene-based aerogel embedded with TiO_2 nanoparticles and MoS_2 nanosheets by a facile one-pot hydrothermal process.[11] The as-prepared MoS_2/P_{25}/graphene aerogel exhibited enhanced light absorption, efficient charge separation and photocatalytic activity. Wu reported that Fe_3O_4 nanoparticals were supported on graphene sheets via a hydrothermal process and fabricated a Fe_3O_4/N-GAs 3D monolithic hybrid with excellent electrochemical activity for the oxygen reduction reaction (ORR) in alkaline electrolytes.[12]

In addition, nitrogen-doped graphene had been widely studied last few years, which was because that incorporating nitrogen atoms into graphene could tailor the electronic structure of graphene and improve its electrochemical performance. So far, several approaches, such as chemical vapor deposition (CVD),[13] GO annealed with nitrogen precursor,[14] GO hydrothermal treatment method,[15] wet chemical reaction method,[16] and plasma treatment method,[17] had been employed to prepare N-doped graphene. However, many of these approaches required either toxic nitrogen precursors or rigorous conditions and special instruments. Among these methods, the hydrothermal method was a facial and efficient way to acquire the N-doped graphene aerogels (NGAs). Melamine is a commercially available, cheap and non-toxic chemical. Besides, the nitrogen content of melamine is 66.7 wt.%, which is much higher than those of other nitrogen sources, such as urea,[18] pyrrole,[19] ethanediamine[20] and so on. Moreover, the controllability of the porous structure and the surface area of the N-doped graphene aerogel, could make obvious influences on its electrochemical performance.[21] Thus, it is desirable to investigate the effect of melamine on structure parameters, such as the porous size and the surface area of NGAs.

Herein, we used the melamine as nitrogen-doped agent to fabricate the N-doped graphene aerogels via a self-assembly process by one-pot hydrothermal method. The synthesized NGAs could have the surface area as large as 992 m^2/g. Especially, it was found that the porous structure and specific capacitance of NGAs could be adjusted by the change of the melamine/GO mass ratio. Moreover, the electrochemical properties of the NGAs were investigated in detail, and obtained results revealed that the NGAs could be a promising candidate for N-doped graphene based supercapacitors.

2. Experimental

2.1. Preparation of Nitrogen-doped Graphene Aerogels. In a typical preparation, graphite oxide (GO) was prepared from natural graphite according to Hummers' method. 0.3 g GO was dispersed in 60 mL deionized water by ultrasonication for 2 h to acquire the GO dispersion with a final concentration of 5 mg mL^{-1}. 12 mL melamine aqueous solution was added slowly into 18 mL GO dispersion under stirring at 60 °C. Then, the mixture transferred into a 50 mL Teflon-lined autoclave at 180 °C for 12 h. The obtained hydrogels were washed with alcohol and acetone three times in sequence, and dried with supercritical CO_2 to obtain N-doped graphene oxide aerogels (NGOAs). The NGOAs were heated to 900 °C at 5°C/min in N_2 atmosphere and held for 2 h to yield N-doped graphene aerogels (NGAs). NGAs with different melamine/GO mass ratios were named as NGA-1, NGA-2, NGA-3, NGA-4, NGA-5 (mass ratio = 0, 1:20, 1:15, 1:10, and 1:5), respectively.

2.2. Characterization. Field emission scanning electron microscopy (FE-SEM) was carried out in an Ultra 55 field emission scanning electron microscope operated at 15 kV. Transmission electron microscopy (TEM) images and selected area electron diffraction (SAED) patterns were measured on a Libra 200FE transmission electron microscope at 200 kV. X-ray diffraction (XRD) analysis was carried out in X' Pert PRO with Cu Kα radiation at λ = 0.15406 nm. Raman microscopy was obtained in an InVia laser Raman spectrometer with λ = 514.5 nm. Specific surface area was characterized by nitrogen adsorption/desorption measurement (AR-JW-BK112).

2.3. Electrochemical Measurements. The electrochemical properties of NGAs were tested in a three-electrode system at room temperature with 0.1 M KOH aqueous solution as the electrolyte. A Pt wire and a saturated calomel electrode (SCE) were used as the counter and reference electrodes, respectively. To prepare the working electrode, NGAs, acetylene black

and polytetrafluoroethylene (PTFE) with a weight ratio of 8:1:1 were pasted on nickel foam to form a homogeneous film. The amount of active materials loading for a single electrode was about 1 mg. The two-electrode system were prepared by pressing a mixture of 80 wt% NGA-3, 10 wt% acetylene black and 10 wt% PTFE on nickel foil and then drying at 60℃ for 12 h. The capacitor was assembled into a two-electrode system, in which the two electrodes were separated by a polypropylene membrane. All cyclic voltammetry (CV), galvanostatic charge/discharge and electrochemical impedance spectroscopy (EIS) of NGAs were studied on a CHI660D electrochemical workstation (Shanghai, China).

3. Results and discussion

3.1. Structure Characterizations.

In the actual experiment, when the melamine aqueous solution was gradually added to the GO solution, the melamine molecular adhered to GO sheets to form brown precipitate. Then, it was transferred into a 50 mL Teflon-lined autoclave at 180 °C for 12 h and GO sheets was self-assembled to form three-dimensional GO aerogels. It had been reported that the weak interaction between graphene sheets, such as van der Waals force, hydrogen bonding and π-π interaction, were the driving force to form three-dimensional porous network structure.[10] As seen from the possible synthesis process illustrated in Scheme 1, when the melamine was added into the GO solution under the hydrothermal condition, the NH_2 groups in melamine moleculars could interact with the hydroxyl or carboxylic acid groups on GO sheets to form hydrogen bonds between melamine molecules and GO sheets. Thus, the melamine molecules inserted into the graphene layers. After pyrolyzed in a tubular furnace at 900 °C for 2 h in a N_2 atmosphere, most of oxygen-containing groups on graphene sheets were removed and nitrogen atoms were doped into the graphene aerogel.

The morphology and structure of NGAs were revealed by SEM and TEM observations. As shown in Figure 1a, the NGAs all had a well defined shape and it could be found that their volume became large with increase of the melamine/GO mass ratio. Correspondingly, the SEM images showed a significant change of their morphology and structure. As seen from Figure 1b-f, when the melamine/GO mass ratio increased, the graphene layers became more loose, rather thin and wrinkled. Moreover, the gradually loose structure of NGAs led to the decrease of their density from 33.9 to 17.2 mg cm^{-3} (Table 1). This could be because that the hydrogen bond between melamine molecules and GO sheets prevented GO sheets from

self-stacking and allowed the sufficient assembly of GO sheets into the large volume.[22] Therefore, the change of the morphology and structure between different NGAs revealed that melamine could suppress the stacking of GO sheets. Furthermore, as shown in the low-magnification TEM image (Figure 2a), thin wrinkles and folds revealed that the graphene sheets in three dimensional structure of NGAs were flexible. Meanwhile, there was a more visible reflection in the high-resolution TEM (Figure 2b) and it exhibited that the thin walls of NGAs typically consisted of only 4-6 layers of graphene sheets. Moreover, the SAED pattern (Figure 2c) showed that the inner circle was brighter than the outer one, which indicated that NGAs were composed of multilayer graphene sheets and was consistent with the TEM observation.[23]

The XRD pattern (Figure S1a) showed that the interlayer distance of NGAs was calculated to be 3.66 Å, which was much lower than that of GO (8.31 Å) but slightly higher than that of natural graphite (3.37 Å).[24] These results revealed the presence of few-layer stacked graphene sheets and the recovery of a graphitic crystal structure.[25] The broad XRD peak of the NGAs further indicated the disordered stacking of graphene sheets. This demonstrated that the framework of the NGAs was indeed composed of few-layer stacked graphene sheets, which agreed with the results of the TEM and SAED pattern.

Raman spectroscopy is a useful tool to characterize the structure and quality of carbon materials. Specially, it could identify the disordered degrees of graphene. It is known that the Raman spectrum of the pristine graphite displays only a prominent G peak.[26] The Raman spectra (Figure S1b) of NGAs and NGOA contained both D bands (the A_{1g} symmetry mode) at about 1353 cm^{-1} and G bands (the E_{2g} mode of the sp^2 carbon atoms) at about 1597 cm^{-1}.[27] The appearance of D band is due to the defects which were introduced into graphene layers when graphite was oxidized and exfoliated in the GO synthesis. In addition, it could be seen that NGAs exhibited slightly increased D/G intensity ratios (I_D/I_G from 0.795 to 0.865) compared to that of the NGOA (I_D/I_G was 0.698). It was attributed to an increase in the number of smaller graphene domains after partial removal of the oxygen moieties, which led to the decrease in the average size of the sp^2 domains upon the reduction of the NGOA. This phenomenon is usually observed in the Raman spectra of reduced GO.

X-ray photoelectron spectroscopy (XPS) characterizations were performed to analyze the nitrogen bonding configurations in NGAs. In the C1s spectrum (Figure 3a) of the NGA-5, the

strong peak at 284.6 eV corresponded to sp^2 carbon atoms, which indicated most of carbon atoms were in the form of conjugated honeycomb-lattice, and the peaks at 285.8, 287.7 and 289.7 eV were attributed to C–N, C=O and COOH, respectively.[28] Furthermore, the bonding configurations of nitrogen atoms in the NGA-5 were characterized by N1s spectra (Figure 3b). The low binding energy peaks at 398.1 and 399.9 eV were assigned to pyridine-like N and pyrrole-like N,[29] respectively, and the high binding energy peak at 402.2 eV was commonly attributed to pyridine-N-oxide.[30, 31] In a word, the C1s and N1s spectra confirmed that nitrogen atoms had been effectively incorporated into the carbon–carbon bonds of graphenes.

3.2. Electrochemical Properties.

Based on the above structure characterizations of NGAs, it could be speculated that the combination of three dimensional porous networks and the N-doping behavior would endow the NGAs with excellent electrochemical performances. Hence, the electrochemical performances of NGAs were evaluated by cyclic voltammetry (CV), galvanostatic charge/discharge and electrochemical impedance spectroscopy (EIS) techniques in 0.1 M KOH aqueous solution. As shown in Figure 4a, CV curves of all the NGAs exhibited the rectangle shape and good symmetry at the scan rate of 10 mV/s, indicating their double-layer capacitor performance. It was worth to notice that all the CV curves of NGA-2 to NGA-5 had a pair of redox peaks, but NGA-1 only had a weak reductive peak at about -0.1V. In accordance with the XPS analysis, the reductive peak in the CV curve of NGA-1 might be due to the electrochemical reactions of the residual oxygen-containing groups on graphene.[32] As for NGA-2 to NGA-5, the redox peaks are plausible attributed to the pseudocapacitive reaction of the nitrogen groups incorporated into the carbon–carbon bonds of graphene. Pyridinic nitrogen as an electron donor in the graphene layer could easily attract the protons (H^+, K^+) to the electrode surface[33] and the pseudocapacitive interactions occured. The pseudocapacity from the redox reaction could make a contribution to the total capacitance of NGAs.

The galvanostatic charge/discharge curves of NGAs were demonstrated in Figure 4b and it could be found that the charge curves of NGAs were almost symmetric to their corresponding discharge counterparts, demonstrating the high reversibility. The specific capacitances (C_a) were calculated according to $C_a = (It)/(mV)$, where I is the constant discharge current, t is the discharge time, V is the potential window, and m is the mass of the

active material in the electrode.[34] The C_a values of all NGAs at current densities of 0.5, 1, 2, and 5 A/g and the comparison of C_a values at 0.5 A/g were exhibited in Figure 5c and d. As seen from Figure 4c, it could be seen that C_a values of all NGAs gradually decreased with the increase of the current density from 0.5 to 5 A/g. This could be attributed that at a low current density of 0.5 A/g, the K^+ ion can easily diffuse into almost all available space of the NGAs, leading to a sufficient insertion reaction. However, increasing the current density has a remarkable impact on the diffusion of K^+ into the material. At a high current density of 5 A/g, the K^+ ion can only approach the outer surface of the NGAs and the material located in the deep space has little contribution to the electrochemical capacitive behavior. Furthermore, as seen from Figure 4d, the C_a increased first and then decreased with the increase of melamine/GO mass ratios. When the mass ratio was from 0 to 1:15, on one hand, the doped nitrogen atom in graphene lattices could advance electrochemical activity. The pyridinic-N and pyrrolic-N had the larger binding energy with K^+, leading to a number of ions to be accommodated on the electrode surface.[20] Thus, the capacitance performance was enhanced. On the other hand, the stacking degree of graphene layers reduced with the melamine addition, which made graphene sheets expose more wrinkles and folds to provide more active sites. However, the C_a showed a downward trend when the ratio further increased from1:15 to 1:5. As for porous carbon materials, the C_a was significantly influenced by the specific surface area.[35, 36] The BET surface areas were investigated by N_2 adsorption/desorption measurements (Figure S2) and listed in Table 1. It could be seen that the BET surface areas of NGA-1, NGA-2 and NGA-3 were 992, 934 and 953 m^2/g, respectively but those of NGA-4 and NGA-5 reduced to 867 and 852 F/g. Although the effective N-doping could improve the C_a of NGAs, the excessive melamine worked as swelling agent for leading to the formation of the large volume. The increase of macropores structures in NGA-4 and NGA-5 was not beneficial for the enhancement of their specific surface areas. It might be the reason why the C_a showed a downward trend when the ratio further increased from 1:15 to 1:5. Thus, it could be revealed that the specific capacitance of NGAs was attributed to the synergistic effect of the doped-N level and the specific surface area, which was decided by the porous structure of NGAs. As a result, the present results demonstrated that the NGA-3 was the optimal candidate for the supercapacitor materials.

In order to further illustrate its electrochemical performance, the CV curves,

galvanostatic charge/discharge curves, specific capacitance curve and cyclic curve of NGA-3 were shown in Figure 5. Figure 5a exhibited the CV curves of NGA-3 at different scan rates. It could be seen that all the CV curves had a rectangle shape and no significant change with the increase of the scan rate, demonstrating its excellent rate capacity. The C_a was calculated according to formula $C_a = (\int IdV)/(m\Delta V\upsilon)$ in CV tests. Here, I is the response current density, V is the potential window, m is the mass of active material and υ is the scan rate.[1] The specific capacitances of NGA-3 were 93, 87, 79, and 65 F/g at different scan rates of 5, 10, 20 and 50 mV/s, respectively. The galvanostatic charge/discharge curves at current densities of 0.5, 1, 2, and 5 A/g were demonstrated in Figure 5b. The charge curve of NGA-3 keep symmetric well to its corresponding discharge counterpart when the current density increased. The time of the charging−discharging procedure increased gradually with the decrease of the current density, which is attributed to the sufficient insertion or release of K^+ during the charging and discharging steps. The specific capacitance of NGA-3 at different current densities in the range 0.5 to 40 A/g was demonstrated in Figure 5c. The C_a values calculated from discharge curves were 116, 101, 91, 86, 75, 66, 62, 58, 57.4 and 56.5 F/g at discharge current densities of 0.5, 1, 2, 5, 10, 20, 25, 30, 35 and 40 A/g, respectively. It could be seen that the capacitance gradually decreased with the increase of current densities, which is usually observed in the electrochemical tests. Even so, it could be seen that the capacitance still kept a relatively stable value after the current density increased to 10 A/g. The electrochemical stability of NGA-3 was also investigated in the range of -0.8 to 0.2 V in 0.1 M KOH aqueous solution (Figure 5d). Its special capacitance almost retained 94% of the initial capacity after 1000 charge-discharge cycles at the current density of 1 A/g. What's more, the capacitance retention just dropped to 92.5% after 5000 charge-discharge cycles at the current density of 2 A/g (Figure S4). The good capacitance retention suggested that the NGA-3 had outstanding electrochemical stability. The electrode conductivity of NGA-3 was characterized by the electrochemical impedance spectroscopy (EIS) measurement. Herein, Nyquist plots were used to analyze EIS properties. In Figure S3, the Nyquist plots of NGA-1 and NGA-3 exhibited sloping lines in the low-frequency region and semicircle-shaped curves in the high-frequency region. In the low-frequency region, the almost vertical lines of both NGA-1 and NGA-3 affirmed their perfect capacitive behaviors. The real-axis intercept in the high-frequency region is considered to be the equivalent series resistance (ESR) of the cell, which determines

the charged/discharged rate of the cell, that is power capability.[37, 38] Obviously, the ESR of NGA-3 was lower than NGA-1, indicating that NGA-3 had the better electrode conductivity. This might be because that nitrogen atoms in graphene lattices could tailor local electronic structures, which is beneficial to enhance the band between the nitrogen atoms and K^+ ions in the solution, resulting in plentiful K^+ ions accommodated on the electrode surface.[29]

Furthermore, a two-electrode system was also used to test the electrochemical performance of the supercapacitor test cell of NGA-3. The CV curves, galvanostatic charge/discharge curves, Nyquist plot, and cyclic performance of NGA-3 were shown in Figure S5. The CV curves (Figure S5a) at different scan rates were rectangular-like shape, which was ascribed to the electric double layer capacitance. The galvanostatic charge/discharge curves at different current densities were shown in Figure S5b. At the current density of 0.2 A/g, the specific capacitance of the cell was estimated as 55 F/g. The cyclic performance of the cell was investigated by CV test at the scan rate of 20 mV/s and its special capacitance retained 84% and 62% of the initial capacity after 1000 and 5000 cycles, respectively (Figure S5c). Moreover, the Nyquist impedance plot in Figure S5d exhibited that NGA-3 possessed a higher ESR value of the cell than three-electrode system, which was mainly attributed to the large internal resistance of the cell. This was also the reason why the electrochemical performance of the two electrode full cell was not comparable to that of the three-electrode system.

As a result, own to its excellent specific capacitance and outstanding cycling stability, the NGA-3 would have a promising potential application of electrode materials in supercapacitors.

4. Conclusion

In summary, we first synthesized N-doped graphene aerogels by using GO and melamine via a hydrothermal process. The pore structure and capacitive performance of NGAs could be controlled by tuning the melamine/GO mass ratio. The synthesized NGA-3 showed a specific capacitance of 116 F/g at the discharge current density of 0.5 A/g and also retained 94% of its initial capacitance after 1000 cycles. The enhanced electrochemical performance could be attributed to the synergistic effect of the doped-N level and the specific surface area, which was decided by the porous structure of NGAs. Our results would open up a facial way for the controllable synthesis of N-doped graphene aerogel materials with excellent electrochemical

performance for supercapacitors.

Acknowledgements

This research was financially supported by the National Natural Science Foundation of China (Grant No. 51502274), the Open Project of State Key Laboratory Cultivation Base for Nonmetal Composites and Functional Materials (11zxfk26), the Postgraduate Innovation Fund of Southwest University of Science and Technology (No.14ycx008), the Science and Technology Development Foundation of China Academy of Engineering Physics (2015B0302003), and the Project Funded by China Postdoctoral Science Foundation (2015M572499).

References

1. J. Zhu and J. He, *ACS applied materials & interfaces*, 2012, 4, 1770-1776.
2. Y. Xue, B. Wu, Y. Guo, L. Huang, L. Jiang, J. Chen, D. Geng, Y. Liu, W. Hu and G. Yu, *Nano Res.*, 2011, 4, 1208-1214.
3. L. Xiao, D. Wu, S. Han, Y. Huang, S. Li, M. He, F. Zhang and X. Feng, *ACS applied materials & interfaces*, 2013, 5, 3764-3769.
4. F. Ghaemi-Oskouie and Y. Shi, *Curr Rheumatol Rep*, 2011, 13, 160-166.
5. X. Wang, J. Wang, D. Wang, S. Dou, Z. Ma, J. Wu, L. Tao, A. Shen, C. Ouyang, Q. Liu and S. Wang, *Chemical communications*, 2014, 50, 4839-4842.
6. R. Wang, Q. Wu, Y. Lu, H. Liu, Y. Xia, J. Liu, D. Yang, Z. Huo and X. Yao, *ACS applied materials & interfaces*, 2014, 6, 2118-2124.
7. J. Goel, K. Kadirvelu, C. Rajagopal and V. K. Garg, *Journal of Chemical Technology & Biotechnology*, 2005, 80, 469-476.
8. K. Y. Kang, B. I. Lee and J. S. Lee, *Carbon*, 2009, 47, 1171-1180.
9. M. A. Worsley, P. J. Pauzauskie, T. Y. Olson, J. Biener, J. H. Satcher and T. F. Baumann, *Journal of the American Chemical Society*, 2010, 132, 14067-14069.
10. Y. Xu, K. Sheng, C. Li and G. Shi, *ACS Nano*, 2010, 4, 4324-4330.
11. W. Han, C. Zang, Z. Huang, H. Zhang, L. Ren, X. Qi and J. Zhong, *International Journal of Hydrogen Energy*, 2014, 39, 19502-19512.
12. Z. S. Wu, S. Yang, Y. Sun, K. Parvez, X. Feng and K. Mullen, *Journal of the American Chemical Society*, 2012, 134, 9082-9085.
13. Z. Jin, J. Yao, C. Kittrell and J. M. Tour, *ACS Nano*, 2011, 5, 4112-4117.
14. Z. Wen, X. Wang, S. Mao, Z. Bo, H. Kim, S. Cui, G. Lu, X. Feng and J. Chen, *Advanced materials*, 2012, 24, 5610-5616.
15. Z. Y. Sui, Y. N. Meng, P. W. Xiao, Z. Q. Zhao, Z. X. Wei and B. H. Han, *ACS applied materials & interfaces*, 2015, 7, 1431-1438.
16. D. W. Chang, E. K. Lee, E. Y. Park, H. Yu, H. J. Choi, I. Y. Jeon, G. J. Sohn, D. Shin, N. Park, J. H. Oh, L. Dai and J. B. Baek, *Journal of the American Chemical Society*, 2013, 135, 8981-8988.
17. T. Odedairo, J. Ma, Y. Gu, W. Zhou, J. Jin, X. S. Zhao and Z. Zhu, *Nanotechnology*, 2014, 25, 495604.
18. H.-L. Guo, P. Su, X. Kang and S.-K. Ning, *Journal of Materials Chemistry A*, 2013, 1, 2248-2255.
19. Y. Zhao, C. Hu, Y. Hu, H. Cheng, G. Shi and L. Qu, *Angewandte Chemie*, 2012, 124, 11533-11537.

20. P. Chen, J.-J. Yang, S.-S. Li, Z. Wang, T.-Y. Xiao, Y.-H. Qian and S.-H. Yu, *Nano Energy*, 2013, 2, 249-256.
21. S. M. Jung, D. L. Mafra, C. T. Lin, H. Y. Jung and J. Kong, *Nanoscale*, 2015, 7, 4386-4393.
22. M. Chen, C. Zhang, X. Li, L. Zhang, Y. Ma, L. Zhang, X. Xu, F. Xia, W. Wang and J. Gao, *Journal of Materials Chemistry A*, 2013, 1, 2869.
23. X. Wu, J. Zhou, W. Xing, G. Wang, H. Cui, S. Zhuo, Q. Xue, Z. Yan and S. Z. Qiao, *Journal of Materials Chemistry*, 2012, 22, 23186.
24. X. Zhang, Z. Sui, B. Xu, S. Yue, Y. Luo, W. Zhan and B. Liu, *Journal of Materials Chemistry*, 2011, 21, 6494.
25. T. Wang, L. Wang, D. Wu, W. Xia, H. Zhao and D. Jia, *Journal of Materials Chemistry A*, 2014, 2, 8352.
26. F. Tuinstra and J. L. Koenig, *The Journal of Chemical Physics*, 1970, 53, 1126-1130.
27. F. López-Urías, R. Lv, H. Terrones and M. Terrones, in *Graphene Chemistry*, John Wiley & Sons, Ltd, 2013, DOI: 10.1002/9781118691281.ch9, pp. 183-207.
28. Z. Wang, Z. Tang, Z. Han, S. Shen, B. Zhao and J. Yang, *RSC Adv.*, 2015, 5, 19838-19843.
29. D. Hulicova-Jurcakova, M. Seredych, G. Q. Lu and T. J. Bandosz, *Advanced Functional Materials*, 2009, 19, 438-447.
30. F. Xu, M. Minniti, P. Barone, A. Sindona, A. Bonanno and A. Oliva, *Carbon*, 2008, 46, 1489-1496.
31. M. Zhou, F. Pu, Z. Wang and S. Guan, *Carbon*, 2014, 68, 185-194.
32. D.-W. Wang, F. Li, J. Zhao, W. Ren, Z.-G. Chen, J. Tan, Z.-S. Wu, I. Gentle, G. Q. Lu and H.-M. Cheng, *ACS Nano*, 2009, 3, 1745-1752.
33. D. Hulicova, J. Yamashita, Y. Soneda, H. Hatori and M. Kodama, *Chemistry of Materials*, 2005, 17, 1241-1247.
34. Y.-T. Wang, A.-H. Lu, H.-L. Zhang and W.-C. Li, *The Journal of Physical Chemistry C*, 2011, 115, 5413-5421.
35. G. Gryglewicz, J. Machnikowski, E. Lorenc-Grabowska, G. Lota and E. Frackowiak, *Electrochimica Acta*, 2005, 50, 1197-1206.
36. S. Yoon, J. Lee, T. Hyeon and S. M. Oh, *Journal of The Electrochemical Society*, 2000, 147, 2507-2512.
37. R. Imran Jafri, N. Rajalakshmi and S. Ramaprabhu, *Journal of Materials Chemistry*, 2010, 20, 7114-7117.
38. M. D. Stoller, S. Park, Y. Zhu, J. An and R. S. Ruoff, *Nano Letters*, 2008, 8, 3498-3502.

Table 1. Melamine/GO mass ratio (Ratio), Densities (ρ), Surface Areas (SA) and Capacitances for all samples.

sample	Ratio	ρ (mg cm^{-3})	SA (m^2/g)	C_a (F/g)[a]
NGA-1	0	33.9	992	80
NGA-2	1:20	22.3	934	82
NGA-3	1:15	18.1	953	116
NGA-4	1:10	17.7	867	73
NGA-5	1:5	17.2	852	55

a. C_a was calculated according to galvanostatic charge/discharge curves at the current density of 0.5 A/g.

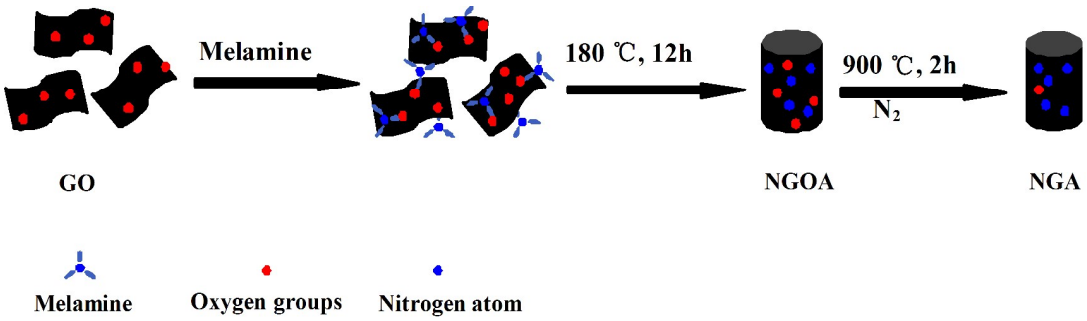

Scheme 1. Schematic illustration of the synthesis of NGAs.

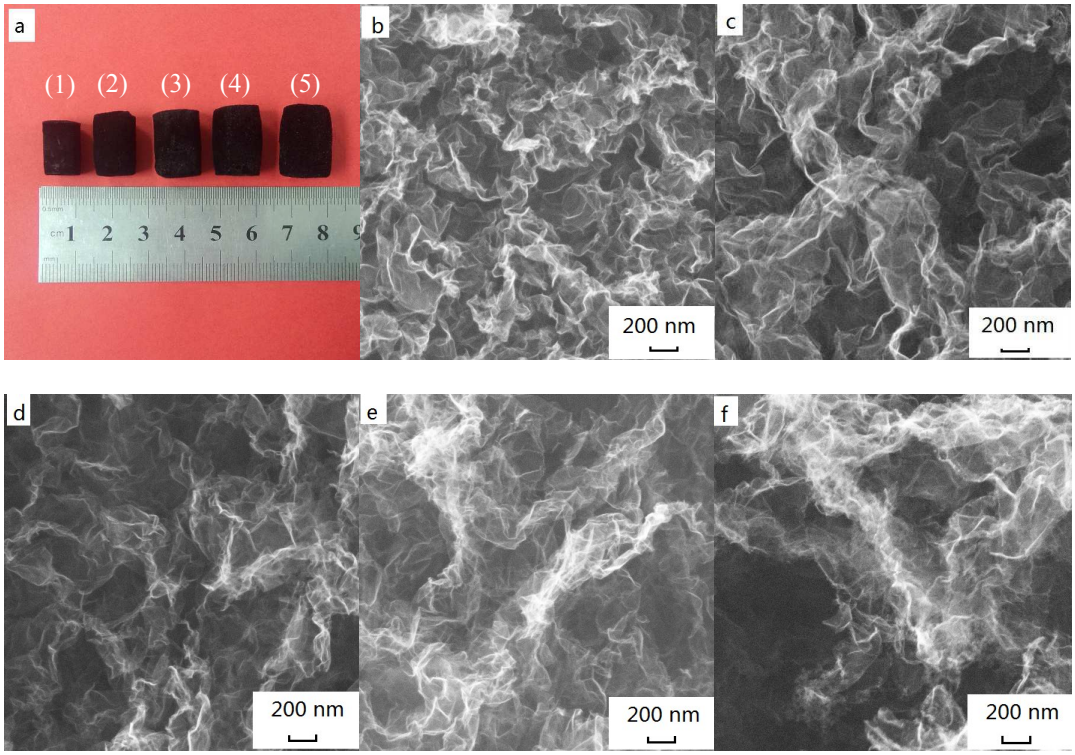

Figure 1. Digital photographs (a) and SEM images of NGA-1 (b), NGA-2 (c), NGA-3 (d), NGA-4 (e), and NGA-5 (f).

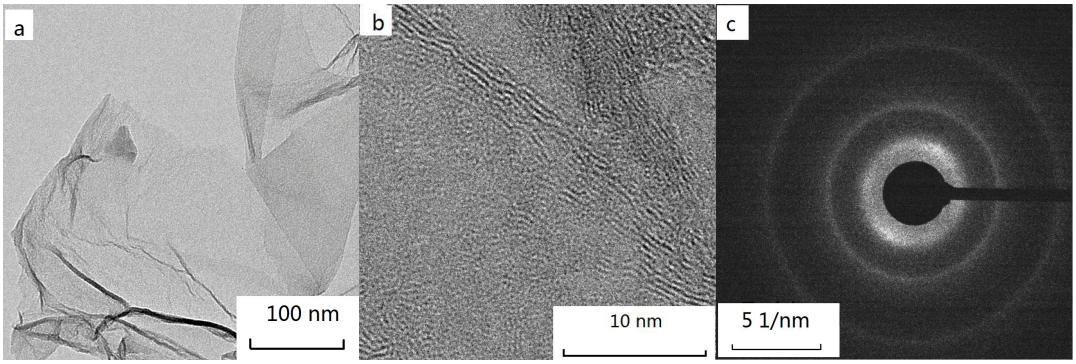

Figure 2. Low-magnification TEM image (a), high-resolution TEM image (b) and selected area electron diffraction (SAED) pattern (c) of NGA-3.

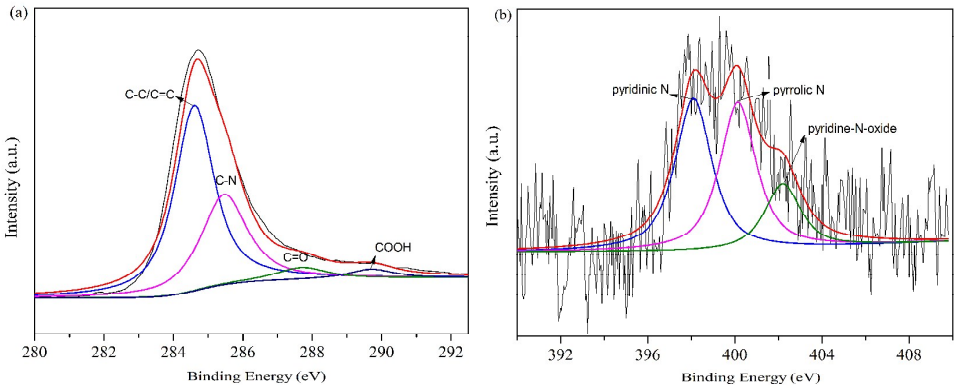

Figure 3. C1s XPS (a) and N1s XPS (b) spectra of NGA-5.

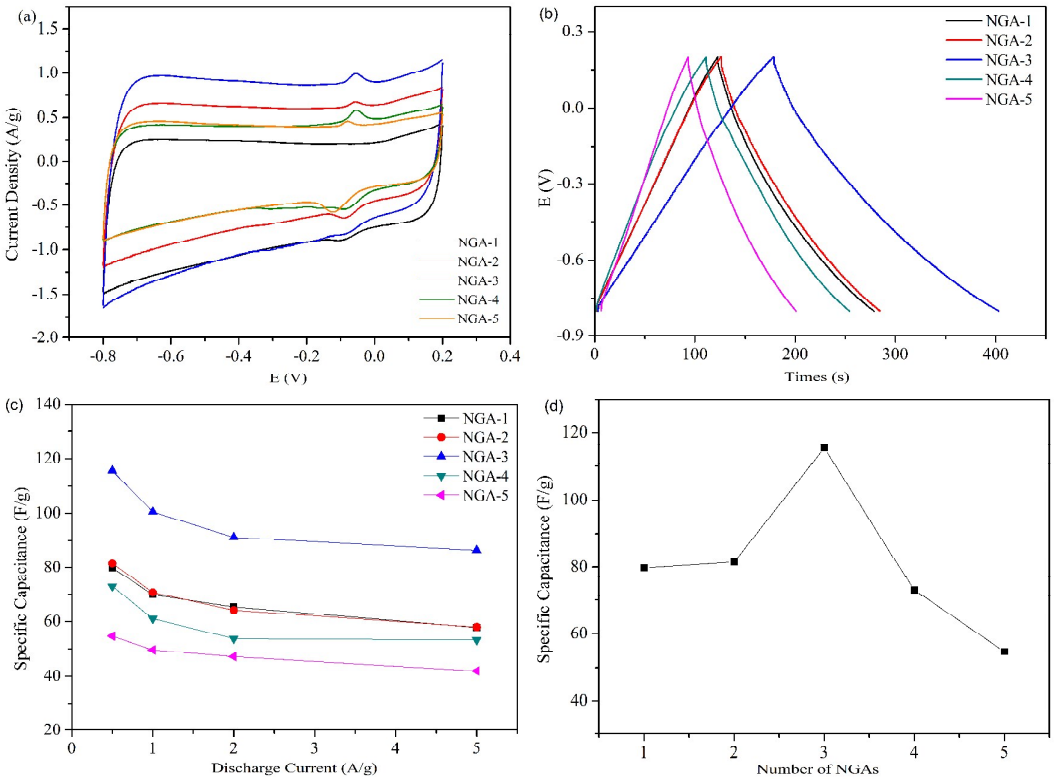

Figure 4. CV curves at 10 mV/s (a), Galvanostatic charge/discharge curves at the current density of 0.5 A/g (b), C_a at different current densities of 0.5, 1, 2, and 5 A/g (c), and C_a comparison of all the NGAs at the current density of 0.5 A/g (d).

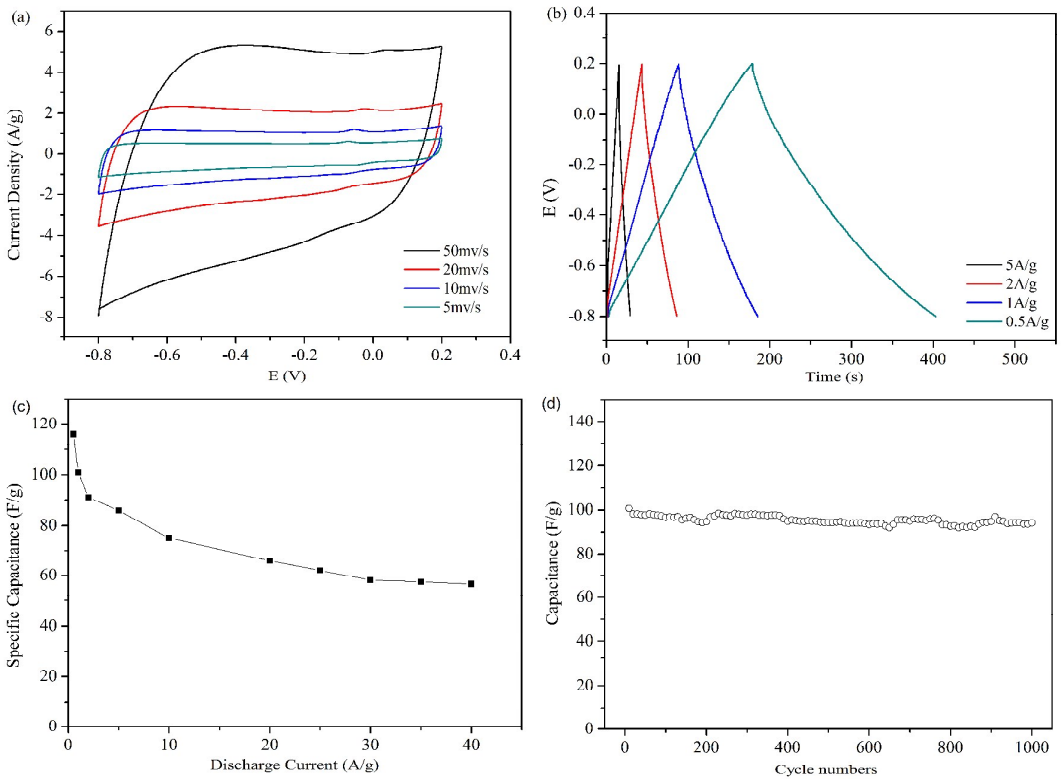

Figure 5. CV curves (a), galvanostatic charge/discharge curves (b), specific capacitance at different current densities in the range 0.5 to 40 A/g (c) and cyclic performance (d) of NGA-3.